1   **Volumetric changes of mud on Mars: evidence from laboratory simulations**

2   P. Brož[1,2], O. Krýza[1,2], V. Patočka[3], V. Pěnkavová[4], S. J. Conway[5], A. Mazzini[6], E. Hauber[7], M. E. Sylvest[2],

3   and M. R. Patel[2,8]

4   [1] Institute of Geophysics of the Czech Academy of Sciences, Prague, Czech Republic, petr.broz@ig.cas.cz

5   [2] School of Physical Science, STEM, The Open University, Milton Keynes, UK

6   [3] Charles University, Faculty of Mathematics and Physics, Department of Geophysics, Prague, Czech

7   Republic

8   [4] Institute of Chemical Process Fundamentals of the Czech Academy of Sciences, Prague, Czech Republic

9   [5] CNRS UMR-6112 LPG Nantes, France

10   [6] Centre for Earth Evolution and Dynamics (CEED), University of Oslo, Norway

11   [7] Institute of Planetary Research, DLR, Berlin, Germany

12   [8] Space Science and Technology Department, STFC Rutherford Appleton Laboratory, Oxford, UK

13   # Abstract

14   Subtle mounds have been discovered in the source areas of martian kilometer-sized flows and on

15   top of summit areas of domes. These features have been suggested to be related to subsurface sediment

16   mobilization, opening questions regarding their formation mechanisms. Previous studies hypothesized that

17   they mark the position of feeder vents through which mud was brought to the surface. Two theories have

18   been proposed: a) ascent of more viscous mud during the late stage of eruption and b) expansion of mud

19   within the conduit due to the instability of water under martian conditions. Here we present experiments

20   performed inside a low-pressure chamber, designed to investigate whether the volume of mud changes

21   when exposed to a reduced atmospheric pressure. Depending on the mud viscosity, we observe volumetric

22   increase of up to 30% at the martian average pressure of ~6 mbar. This is because the low pressure causes

instability of the water within the mud, leading to the formation of bubbles that increase the volume of the mixture. This mechanism bears resemblance to the volumetric changes associated with the degassing of terrestrial lavas or mud volcano eruptions caused by a rapid pressure drop. We conclude that the mounds associated with putative martian sedimentary volcanoes might indeed be explained by volumetric changes of the mud. We also show that mud flows on Mars and elsewhere in the Solar System could behave differently to those found on Earth, because mud dynamics are affected by the formation of bubbles in response to the low atmospheric pressure.

Plain Language Summary

Mars is a planet whose surface atmospheric pressure is ~160 times weaker than on Earth. This means that the conditions on the surface of Mars are not supportive to the existence of liquid water as water should boil and evaporate. At the same time, many edifices on the planet's surface that have been previously observed are believed to be the result of mud movement over the martian surface. Therefore it was proposed by many that they should be the result of a process of sedimentary volcanism during which the sediment is mobilized by liquid water. However, until now it remained unclear how the muds of various viscosities would behave under current martian conditions. Here we show that depending on the mud viscosity, volumetric increase of up to 30% might occur. This is because the low pressure causes instability of the water within the mud, leading to the formation of bubbles that increase the volume of the mud mixture. This shows that mud flows on Mars and elsewhere in the Solar System could behave differently to those found on Earth and therefore we might encounter different shapes of edifices formed on Mars by sedimentary volcanism than on Earth.

1. Introduction

On Earth, sedimentary volcanism manifests at the surface as the eruption of fluids (water, gasses and occasionally oil), fine-grained sediments (e.g., clays) and various sized clasts originating from the country

46   rock (Mazzini and Etiope, 2017). The mud mixture erupted onto the surface can have varying viscosity due

47   to the variations in the water/clay ratio and this can affect the sizes, shapes and thicknesses of the resulting

48   mud flows and these final mud volcanoes morphologies (Mazzini and Etiope, 2017). In general, the higher

49   the water content, the lower the viscosity of the mud and vice versa. Therefore, the rheology of the

50   ascending mud is an important factor controlling the way the mud behaves during its eruption and

51   subsequent emplacement. However, while the behavior and the rheology of mud with different viscosities

52   during the emplacement of terrestrial sedimentary volcanism has been previously extensively investigated

53   (e.g., O'Brien and Julien, 1988; Laigle and Coussot, 1997 and references therein), this is not the case for

54   Mars (see Brož et al. [pre-print] for details), nor for other celestial bodies within the Solar System for which

55   sedimentary volcanism has been proposed (e.g., Ruesch et al., 2019). As a result, only limited insight about

56   mud propagation under different environmental properties than prevailing on Earth exist, both from

57   theoretical and experimental point of view (Wilson and Mouginis-Mark, 2014; Brož et al., 2020a,b).

58   　　　　Based on theoretical predictions and results of laboratory experiments done by Bargery et al. (2010)

59   and Wilson and Mouginis-Mark (2014) proposed that the water present in the mud would be unstable and

60   evaporate from the mud flow, ultimately removing the latent heat from the mixture. Hence, the residual

61   water present in the mud mixture would freeze relatively quickly, in a range of hours to days (Wilson and

62   Mouginis-Mark, 2014). Further studies by Brož et al. (2020a,b) experimentally investigated the propagation

63   of water-rich mud in a low-pressure chamber partly simulating the current environmental conditions of

64   Mars. The authors discovered that low viscosity mud flows could propagate over cold (<273 K) and warm

65   (>273 K) surfaces at current martian atmospheric pressure. However, the mechanism of such propagation

66   would be different to that observed on Earth. On Mars, mud propagating over cold surfaces should rapidly

67   boil and freeze due to evaporative cooling (Bargery et al., 2010) forming an icy-crust full of small voids.

68   This leads to propagation in a similar manner to pahoehoe lava flows on Earth (Brož et al., 2020a). Whereas

69   the mud propagating over a warm surface should levitate due to the intense boiling of water before

70   eventually freezing (Brož et al., 2022b). However, as these experiments only studied the behavior of low

71 viscosity mud (12.7 mPa s at ~276 K and 10.7 mPa s at ~296 K), it remained unclear whether an increase

72 in mud viscosity would change the mud behavior.

73   Mud volcanoes on Earth release mud with a wide range of viscosities (Mazzini and Etiope, 2017),

74 and therefore it is reasonable to expect similar variations in the mud extruded on other planetary surfaces

75 to vary as well. Brož et al. (2019) proposed that the large variability of mud-volcano-like edifices in Chryse

76 Planitia on Mars might be the result of such viscosity variations. Since the ability of water vapor bubbles

77 to escape from the mud depends directly on the viscosity of the mixture, the intense boiling caused by the

78 low atmospheric pressure might affect more viscous muds differently than those with a low viscosity. To

79 date, no experimental comparisons have been performed. Inspired by work of Wilson and Head (2017)

80 focusing on the formation of lunar lava foams in association with Irregular Mare Patches (IMPs; Fig. 1a),

81 Brož et al. (2019, 2022) proposed that an analogous mechanism might operate on Mars in association with

82 sedimentary volcanism. The authors argue that low pressure conditions lead to the intense boiling that

83 causes the formation of large quantities of bubbles and their subsequent growth within the mud. If the

84 viscosity of the mud does not allow easy escape for the bubbles, the mud may expand within the feeding

85 conduit towards the end of the eruption (Hecht, 2002; Bargery et al., 2010). This results in small extrusion

86 of a small amount of the remaining fluid from the feeding conduit might occur (Chassefiére and Leblanc,

87 2011; McGowan, 2011; Brož et al., 2019, 2022; De Toffoli et al., 2019, 2021). Brož et al. (2019, 2022)

88 argued that this process might explain the presence of a) subtle mounds observed in the source regions of

89 martian kilometer-sized flows and b) meter-sized knobs rising at the summit areas of kilometer-sized domes

90 and cones. Both features have been proposed to be associated with processes of subsurface sediment

91 mobilization (Fig. 1b,c). However, a competing theory relating the mounds with the ascent of a more

92 viscous mud during the very late stage of eruption was also considered (Brož et al., 2019; 2022). As we are

93 still lacking the critical ground truth, this issue cannot be resolved solely on remote sensing data.
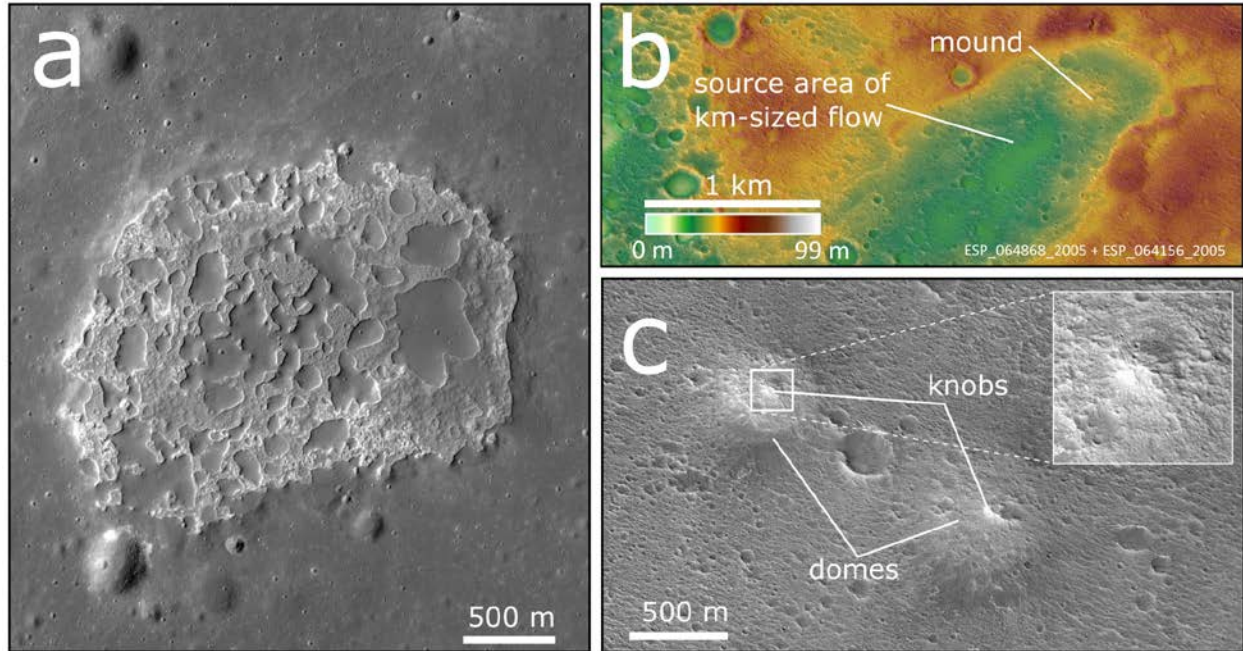
94

Figure 1: Foam examples(a) on the Moon and small mounds (b) and knobs (c) on Mars. a) Ina, the most
known example of lunar Irregular Mare Patches, the width of the image is 3.5 km, Lunar Reconnaissance
Orbiter, NASA, centered at 18.65°N, 5.29°E, b) an example of mound within the source area of kilometer-
sized flow in Chryse Planitia based on DTM generated from HiRISE stereo pair, centered 20.27°N
324.08°E, and c) two domes with central knobs situated within Chryse Planitia, HiRISE
ESP_021748_1990, centered at 18.86°N, 322.63°E.

The goal of this manuscript is to investigate, through analogue modeling, the behavior of various viscous muds under martian pressure conditions. The aim is to understand how the instability of water within such mixtures can affect the volume of the mud sample(s) and to address the following question. Is viscous mud responding differently to intense boiling compared to low viscosity mud? And if so, how does this affect the final morphology of the resulting mud flows as well as associated sedimentary volcanoes on Mars?

2. Experimental setup and methods

2.1. Experimental setup

We performed a set of experiments (see Table 1 for details) using the Mars Simulation Chamber at the Open University (UK). We inserted a $0.38 \times 0.27 \times 0.1$ m sized plastic box filled with a ~10 cm thick layer of natural sand (ø ~200 µm) mixed with water. The temperature of the sand mixed with water was around -20°C in order to limit the infiltration of mud into the sand and to maintain the air temperature below 0°C during the experimental run. To achieve such a temperature, we kept the plastic box inside a freezer for ~2 hours before each experiment. Inside the sand infill was placed a plastic circular container to accommodate 600 ml of mud (Figure 2). Once the experiment started, there was no active cooling of the icy-sandy mixture, hence the mixture slowly warmed up. Note: all experiments were completed before the temperature of the icy-sandy mixture reached the melting point of the water ice.

The temperature of the mud when poured into the container was either 0.5-3°C or 20-22°C (see Table 1 for details). Once the container was filled with the mud, the experiment immediately started. Three different viscosities were tested (see Section 2.2. for details). The first mix contained 50 wt% clay and water (i.e. 1:1 mix, further referred to as "medium"), the second was prepared by mixing 75 wt% clay with 25 wt% water (3:1, further referred to as "high"). And the third one was prepared by mixing 75 wt% water with 25 wt% clay (1:3, further referred to as "low").

The pressure was gradually reduced from 1 bar to 5-7 mbar within a timeframe of minutes (rapid) or in >hour (slow) (see Table 1 for details). In the case of "medium" and "high" viscosity mixtures, each experimental run was done in triplicate to confirm reproducibility. Experiments using "low" viscosity mixture were not done in triplicate because the behavior of such mud was previously studied by Brož et al. (2020a,b) and volumetric changes were not observed. These two experiments were done to verify this observation using the experimental setup and protocol of this study. Experimental runs were recorded by three cameras from different angles (marked as Cam #1-3 on Fig. 2). Cam #2 and Cam #3 had a scale placed

131 in their field of view to enable the measurement of any deformation or volume change. Additionally, three

132 thermocouples were set in the chamber to monitor the temperature of a) the mud (T_{mud}), b) the underlying

133 sandy surface (T_{layer}) and c) the air within the chamber (T_{air}). Data from thermocouples showing thermal

134 evolution of the icy-sandy layer and mud within the container are not discussed further within this paper,

135 however, they are provided on the Zenodo.org depository for those who are interested together with movie

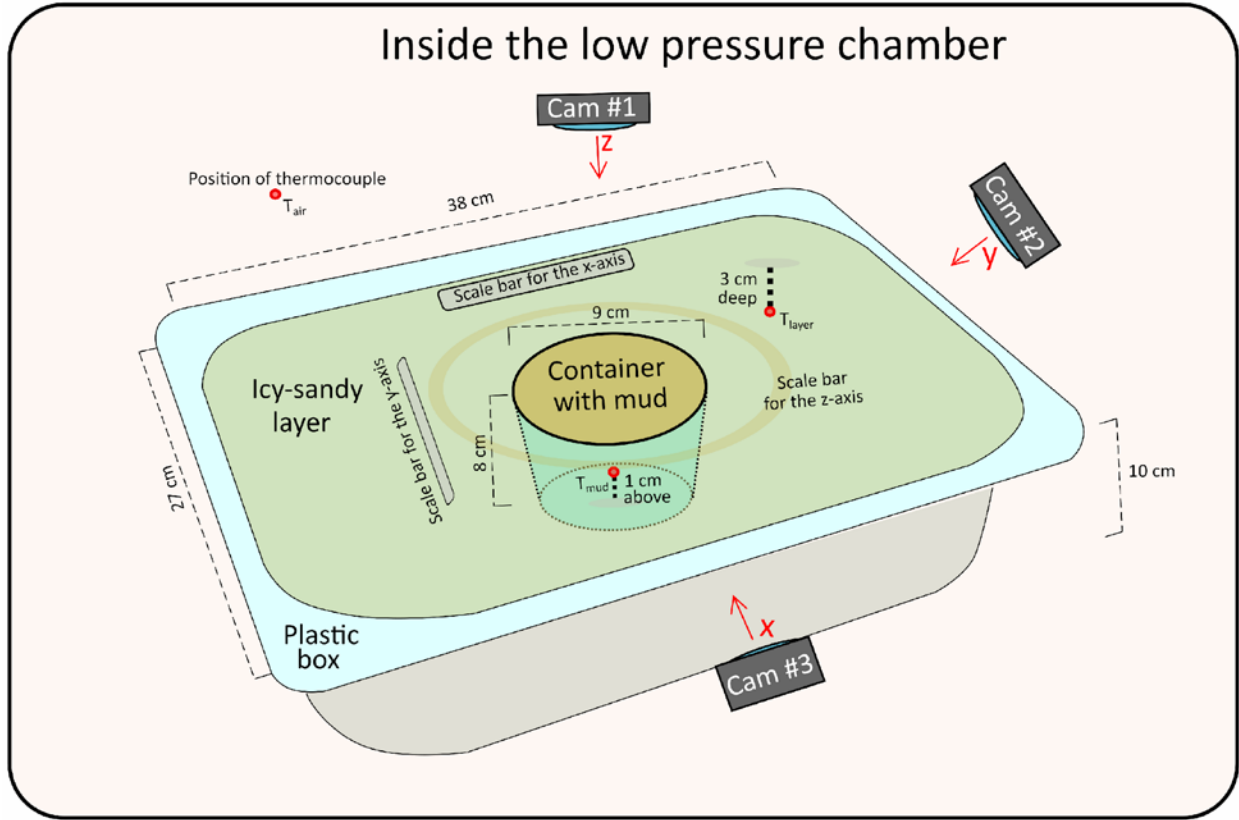136 clips. The experiments did not account for the effect of the lower gravity on Mars as compared to that on

137 Earth.

138

139 *Fig. 2: Schematic illustration showing the experimental setup inside the Mars Simulation Chamber. Marked*

140 *are the positions of the thermocouples, the 3 cameras used to observe each experimental run as well as*

141 *scale bars used to calculate the volumetric changes described in the following subsection.*

142   The mud mixture that we used in the experiments was a mixture of deionised water with 0.1% w/w

143   of dissolved magnesium sulfate salts ($MgSO_4$) and clay content varying depending on the required

144   viscosity. The magnesium sulfate salt was added into the water to achieve salinity enabling it to suspend

145   submillimetre clay particles within low viscosity mixtures (Corradi et al., 1994). This type of salt was

146   previously used in experiments by Brož et al. (2020a,b) and has been detected on the martian surface (Clark,

147   1978; Vaniman et al., 2004; Hecht et al., 2009). Similarly, we also used the same type of clay described by

148   Brož et al. (2020a,b) in their experiments for consistency. Currently, there is no direct in-situ knowledge of

149   which types of clay could be involved in the subsurface sediment mobilization on Mars (Brož et al., under

150   review). The used clay was obtained from the claystone named "Rokle" situated near the town Kadaň

151   (Czech Republic) and operated by the Keramost company. This clay is a bentonite composed of 76%

152   montmorillonite, 23% illite, and 1% kaolinite and formed by alteration of pyroclastic rocks. As explosive

153   volcanism was likely common on Mars (e.g., Brož et al., 2021), to a first approximation this material

154   represents a suitable analogue. The mud mixture was prepared by using a blender for 3 minutes to reduce

155   the presence of clayey aggregates.

Experiment #	Viscosity	Pressure [mbar]*	Temperature of the mud [°C]	Duration of the experiment [min:sec]
1	medium	7	20	4:45
2	medium	7	22	60:00+
3	medium	6	1	4:30
4	medium	6	20	60:00+
5	medium	6	21	5:00
6	medium	6	0.6	3:40
7	medium	6	1	60:00+
12	medium	6	1	60:00+

17	medium	6	21	4:40
18	medium	6	1	3:50
19	medium	6	0.5	60:00+
20	medium	6	15	60:00+
24	high	6	14	60:00+
25	high	6	16	3:50
26	high	6	18	3:40
27	high	6	0.2	3:20
28	high	6	17	3:30
29	high	6	13	60:00+
30	high	6	0.1	60:00+
31	high	6	1.5	3:30
32	high	6	0.6	60:00+
33	high	6	16	60:00+
34	high	6	0.3	3:30
35	high	6	0.5	60:00+
36	low	5	18.5	60:00+
37	low	5	16.3	2:30

* Lowest value of the pressure drop that had been reached.

156   *Table 1: Summary of measured and controlled variables for each experimental run. Experimental runs*

157   *with pressure drops that took more than 60+ minutes are referred to as 'slow' and those that took only*

158   *minutes are referred to as 'fast'.*

2.2. Mud viscosity

Bentonite suspensions containing $MgSO_4$ have complex rheological behavior. These non-Newtonian fluids exhibit both shear thinning behavior (viscosity decreases with increasing applied shear stress) and thixotropy (viscosity decreases in time when constant shear stress is applied). More viscous samples can also exhibit yield stress (below this stress, suspension behaves as an elastic solid, the yield stress should be exceeded in order to induce flow). For these reasons, it is convenient to describe the flow behavior of the used muds using flow curves measured in a reasonable range of shear rates in steady state (avoiding influence of thixotropy). Static yield stress (measured transient between solid and liquid behavior) can be given as an additional information in the case of the "high" consistent mud. The measured viscosity values are presented in Figure 3 and details about measurements are provided in Supplementary materials. However, the low pressure applied during experiments in Mars Simulation Chamber influences the viscosity of muds. The mud viscosities will be much lower than that measured under pressure 1 bar. The ratio between viscosities remains in the trend low < medium < high, but values of viscosities and yield stress will go down.
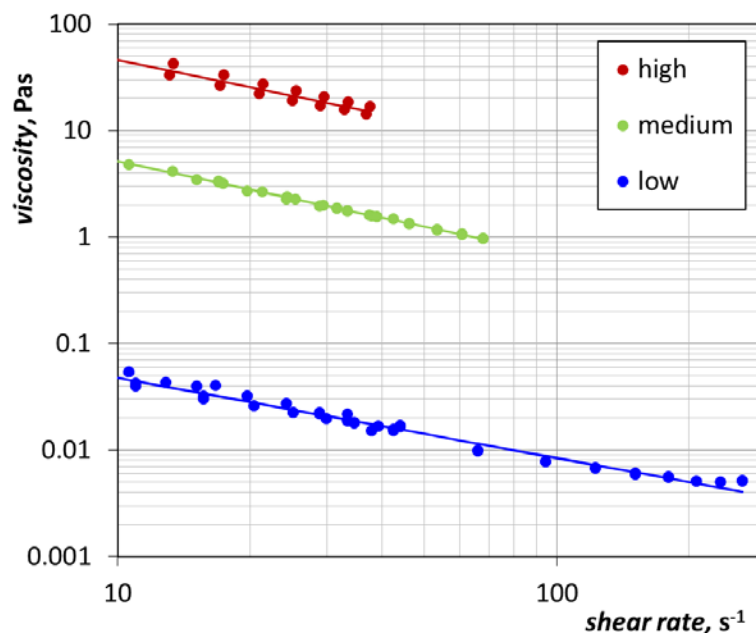
174   *Figure 3. Curves of low, medium and high viscosity aqueous bentonite samples containing 1% MgSO$_4$. The*

175   *lines correspond to power law fits according to Equation 1.1 in Supplementary materials.*

2.3.   Calculation of volumetric changes

177   In order to quantify volumetric changes of the mud samples, we combined information from the

178   calculated velocity fields (employing Cam#1 videos of the individual experiments) and from orthogonally

179   captured images (Figure 4).

180   First we calculated the velocity field of expanding mud (mud bulge) from the top view (z-plane)

181   by 2D PIV method using PIVlab (MatLab open source toolbox; Thielicke and Stamhuis, 2014). This

182   velocity field F is a projection from 3D space but reflects real plane components of the velocity vectors

183   (Figure 4a). To identify the timing of the most rapid volumetric changes, we calculated the 2D divergence

184   field inside the circular area that overlaps the mud sample (Figure 4a).

185   The classical 3D expression of the Gauss' theorem can be directly used to estimate information about

186   volumetric changes based on the 3D divergence field or 2D surface flux of the area. However, in our planar

187   (2D) projection, we naturally lose information about the orientation of the vector components

188   (outward/inward-pointing normals) respective to the curved surface of the growing bulge and we simplified

189   the problem to 1D-2D expression. We tested fluxes over an enclosed circle defined ~0.5 cm from the

190   boundary of the container and also divergence inside this circle. For further analysis, we focused exclusively

191   on the volume (surface) part of the Gauss' formula. We calculated integrated and averaged values of

192   divergence in the selected region (blue circle corresponding to the boundary of the container filled by mud

193   in Figure 4a) for each timestep where the velocity field was derived from the experiment movie. The

194   integrated divergence values are typically negative, positive or zero for current timestep and thus

195   correspond to contraction, expansion or steady state of material (blue, red and zero at the Figure 4b). The

196   resulting plot is used to indicate significant volumetric changes and the state of bulge inflation (difference

197   between two plane areas at Figure 4c,d). Note that in a projection this does not correspond to real volumetric
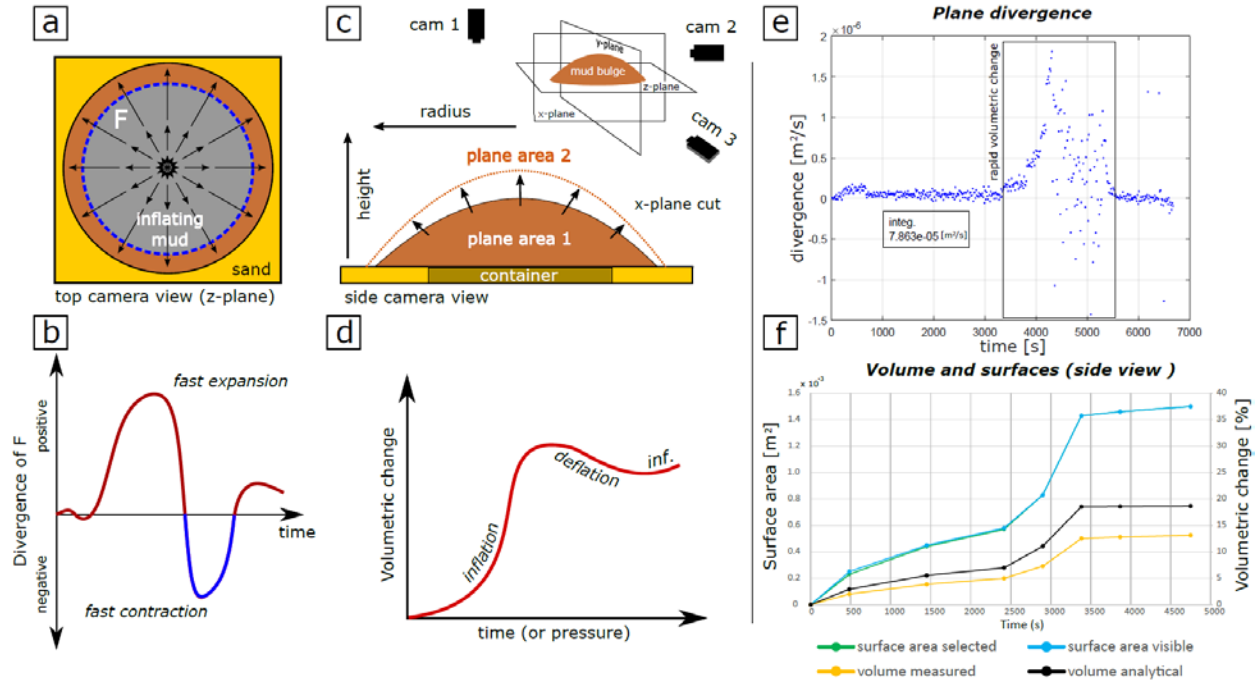
198   change.

199

*Figure 4. Calculations of volumetric changes in our experiments. (a) The velocity field **F** was calculated*

by the 2D PIV method and corresponds to a planar projection (along the z-axis) of an expanding mud

material in 3D (expansion is projected in z-plane). Divergence of this field was calculated in the restricted

region (blue dashed circle) which overlaps the position of the mud source container (the gray area). Arrows

indicate the material movement direction (expansion). Diagram (b): corresponding averaged values from

gray area for all calculated timesteps; maximum and minimum values are related to fast dilatation and

contraction of the mud bulge. (c) The real mud volume above the sandy layer was calculated from

orthogonal projections of the mud bulge and computed for timesteps for which a rapid volume change was

indicated by analysis of the velocity divergence. Here both dimensions and plane areal size of the bulge

projection were used to approximate 3D volume. (d) Example of diagram capturing the volume evolution

against the duration of the experiment or against the ambient pressure. (e) Divergence of the velocity field

integrated in the selected area for each timestep (blue dots). Total time integration is displayed in the small

212 *inset. (f) Diagram of measured surfaces and volumes for selected timesteps (dot values). Volumetric change*

213 *is taken respectively to the initial state of the mud sample (0% change). Both approaches, i) analytical*

214 *construction of idealized half-ellipsoid and ii) calculation from measured plane area, are represented by*

215 *black and yellow curves. Figures e,f, show an example of calculated divergence and volumes during*

216 *experiment #30.*

217 Then we focused on timesteps associated with significant volume changes by the divergence

218 analysis (Figure 4e). For these timesteps, we restored the volume of the mud bulge using the related

219 orthogonal images (this simplification was chosen to resolve the lack of 3D stereoscopic system in the

220 chamber, Figure 4c). Mud bulges were generally symmetric due to controlled geometrical setting and

221 environment during each experiment. Therefore, we used the ImageJ (Fiji) software and calculated the real

222 size of plane projections over the central part of the mud bulge (x-plane), height of the bulge and its radius.

223 Two methods of incremental volume calculation through time were established and compared: a)

224 integration of measured x-plane (y-plane) projection of bulge central section (plane area 1,..2,..n) along $\pi \cdot r$

225 circle; 2) calculation of idealized half-ellipsoid from current radii (in x and y planes) and height. Both

226 approaches gave similar trends and values (typically with 2-9% difference in total change) and an output

227 example is displayed in Figure 4f (plot for experiment #30). In several experiments we also compared x-

228 plane and y-plane measurements, however, the difference was only ~2-3 %. Experiments with deflation

229 and progressive collapse of the bulge are characterized by temporal transition from ellipsoidal to toroidal

230 geometry. The most significant differences between both applied methods then reflect this transition.

231 It should be noted that the above calculations have limitations. Once the central part of the mud body

232 deflated below the original level of the sandy surface, it was not possible to calculate the subsequent

233 volumetric decrease. Likewise, when the rapid boiling and mud eruptions caused ballistic droplets, the

234 divergence calculations were affected by increased number of artifacts in the calculated velocity field.

235 Additionally, it was not possible to quantify the ejected material that was not accounted for during further

236 calculations of total volumetric change. In this case, calculations and measurements were then interrupted.

3. Observations and results

Once the atmospheric pressure started to drop, the initial degassing of the mud was observed. During this initial phase were released the bubbles trapped in the mud during its emplacement. When the pressure dropped below a critical threshold inside the chamber, the mud started to boil (Figs. 5 and 6). The exact value of the boiling threshold was different for each group of experiments as it depended on the temperature of the mud. The hotter the mud was, the sooner it started to boil. During the experiments performed with warm (room temperature) mud, the boiling occurred between 200 to 150 mbar (Figs 5a, 6a), while for the cold mud (1-4°C) it was between 30 to 20 mbar (Fig. 5a,f).
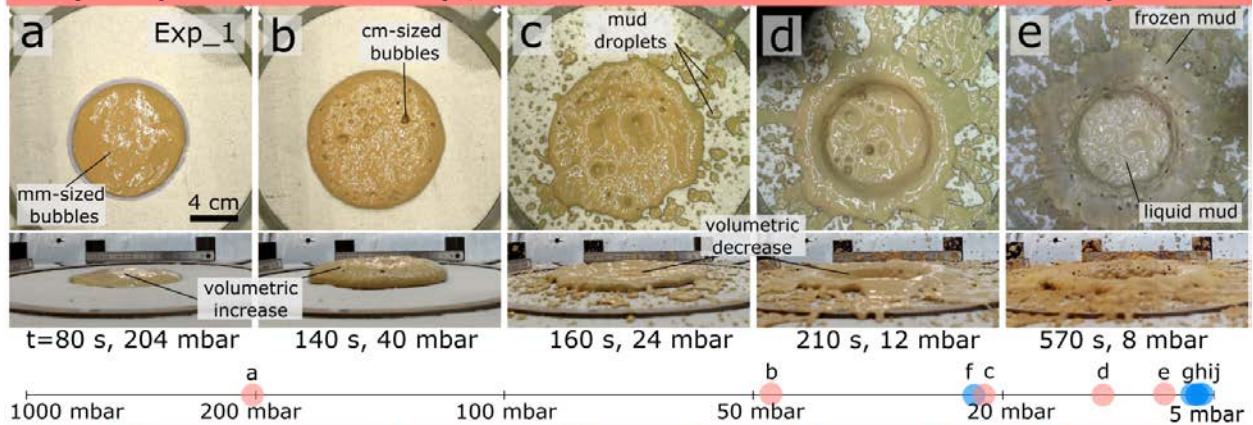
3.1. Medium viscosity mixture

The formation of water vapor bubbles during the initial boiling phases of the medium viscosity mixture was not visible by the naked eye. However, this process could be inferred by the rising of the mud within the container (Figs. 5 and 6). During the pressure drop, small bubbles were conclusively seen on the mud's surface. This gas escape from the mud mixture produced small surface depressions (Figs. 5a,f, 6a). During this stage, the volumetric increase of the mud continued (Fig. 6) in both vertical and horizontal directions beginning to propagate over the icy-sandy surface (Figs, 5b,g, and 6b). Additional pressure drop prompted the size increase of the escaping bubbles from 1-2 mm to up to 10-15 mm (Figs. 5b,g,h, and 6c). While the collapse of small bubbles did not significantly change the surface morphology, alterations were observed during the collapse of large bubbles. Consequently, the smooth surface of the mud became irregular with many knobs and depressions (Figs. 5c,h and 6b). While the formation of large bubbles generally increased the lateral movement of the mud outside of the container, their collapses caused a partial local deflation of the volume (see bottom panels in Figs. 5c,d, 6d or appropriate lines on Fig. 6).

Depending on the mud temperature and the speed of the pressure reduction, the following events observed during the experiments varied. For experiments using mud at room temperature ("warm") and with a rapid pressure drop, significant boiling caused ejection of muddy droplets from the container into

261   the surroundings (see Fig. 5a-f). Such behavior was not observed in other medium viscosity experiments.

262   The muddy droplets were capable of flying dozens of centimeters away from the container (Fig. 5c) along

263   ballistic pathways. At this stage, the lateral movement of the medium-viscosity mud caused by the volume

264   change stopped and the mud reached its maximum surface coverage (Fig. 5c). The volumetric change in

265   the vertical direction, however, continued. Periodically, the mud was inflating and deflating as water vapor

266   bubbles formed, accumulated, and later escaped the mud. This caused repetitive ejection of muddy droplets

267   to the surrounding area. When the pressure reached the intended level (see Table 1 for details), a large

268   bubble formed inside the remaining mud, ejecting a significant amount of material outside the cup. After

269   that, the intensity of boiling decreased and intervals between each phase of mud ejection got longer. When

270   the pressure decreased below 7 mbar, the ejected muddy droplets were rapidly freezing due to evaporative

271   cooling and, after a while, an icy-muddy crust formed over the liquid mud that remained inside the plastic

272   cup. Once the crust covered the entire mud surface, additional boiling and volumetric increase was limited.

273   The maximum volumetric increase reached ~15% for this experimental setup (red dashed line with squares
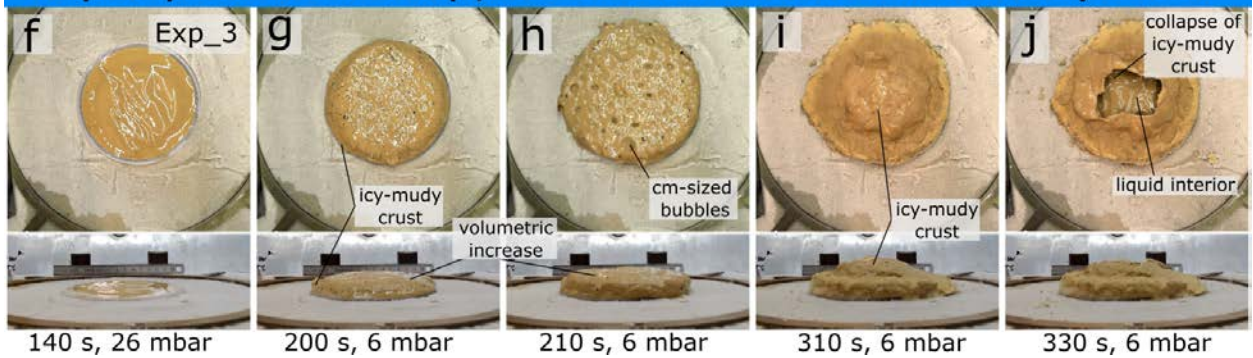
274   in Fig. 6).

Figure 5. Sequence of images from different time steps capturing the behavior of medium viscosity "warm" (top sequence) and "cold" mud (bottom sequence) during rapid pressure drop to 5 mbar. Once the pressure began to drop, intense boiling of the mud occurred, causing a volumetric increase. In the case of warm mud, the formation of a large quantity of bubbles caused significant lateral movement of the mud. Whereas for the cold mud an ice-mud crust formed rapidly, limiting the lateral movement, focusing the volumetric growth in the vertical direction compared to the warm experiments. The boiling of warm mud was more violent, which led to the ejection of mud droplets that were thrown into the surroundings. Finally, the intense production of a large quantity of bubbles also led to episodes of deflation and hence volumetric decrease. Each panel is composed by two figures capturing the experiment from the above (upper image, cam#1) as well as from the side (lower image, cam#2). The axis between the panels captures the pressure value and position of each time step is marked there.

287   The formation of icy-muddy crust differed significantly for the group of experiments using "cold"

288   mud and experiencing a rapid pressure drop (see Fig. 5f-j). The freezing started much earlier than in the

289   warm experiments and caused the formation of an icy-muddy crust on the edges of the volumetrically

290   increasing mud body (Fig. 5g). The crust started to form at the contact of the mud with the icy-sandy surface

291   and propagated upwards. The frozen crust limited the spread of the mud in the horizontal direction for some

292   time. Thus, the volume increase took place mainly in the vertical direction, and only after a few seconds of

293   growth the encircling icy-muddy crust collapsed and the flow quickly spilled laterally over the ice-sand

294   surface (Fig. 5h). This lateral spreading caused a small decrease in the height of the inflated mud sample as

295   the material was spread over a wider area. At the same time, the formation of the ice-mud crust continued,

296   in such a way that the crust grew from the edges towards the center, thereby reducing the area where liquid

297   mud was visible (Fig. 5i). This caused further vertical growth, but at this stage it was centralized in the area

298   where liquid mud was still present on the surface. This meant that while the lateral parts of the mud body

299   no longer increased in volume, the central part grew (Fig. 5i and blue dashed line with squares on Fig. 6).

300   A steep conical edifice formed. The following phase features the collapse of the uppermost part of this

301   conical edifice. This breaching occurred due to the pressure increase within the interior of the bulging body

302   resulting in the exposure of liquid mud remnants . At this point started a new volumetric increase of the

303   liquid mud (Fig. 5j) followed by the development of a new icy-muddy crust. The maximum volumetric

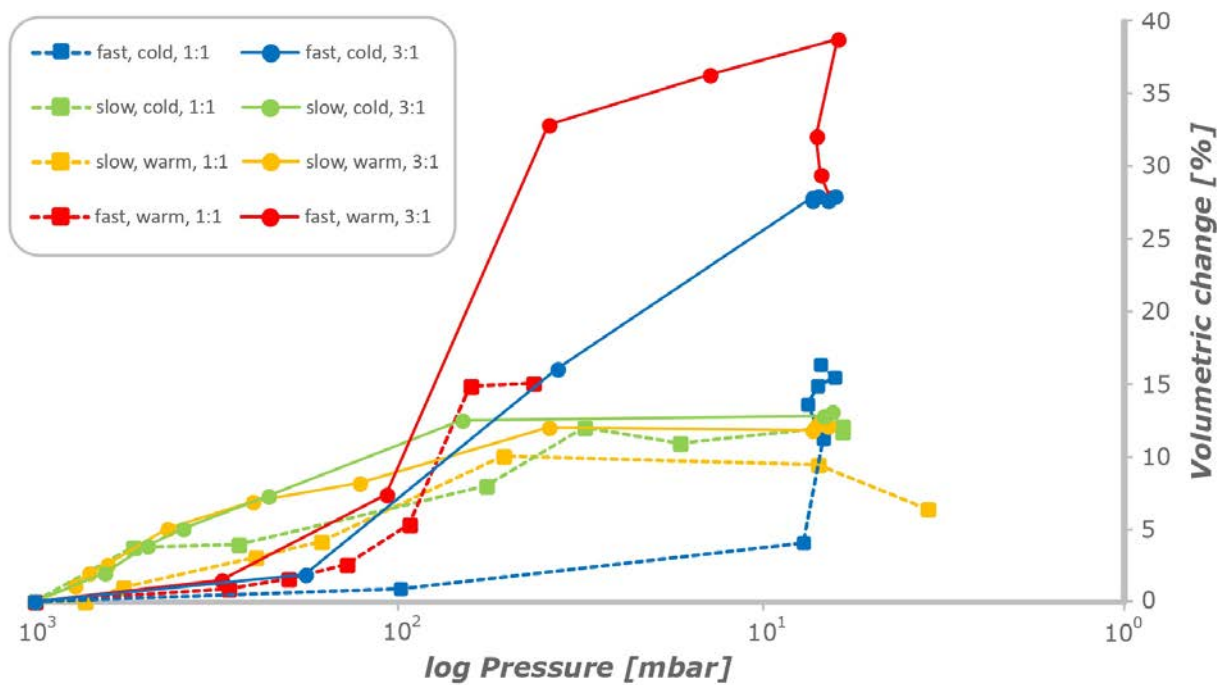304   increase reached ~16.3% for this experimental setup (Fig. 6).

Figure 6: Results of volumetric change measurements.

Different results were obtained exposing warm, medium viscosity mud to a slow pressure reduction (Fig. 7a-e). As the pressure inside the chamber began to decrease, a volumetric increase was observed. Together with sparse millimeter-sized bubbles a number of similarly sized extensional cracks infilled with water were observed to form on the surface (Fig. 7a). When boiling intensified, producing centimeter-sized bubbles (Fig. 7c), the cracks were completely destroyed. The boiling and bubble formation was not as vigorous as for the experiments with a rapid pressure drop and, as a consequence, the ejection of muddy droplets was limited (Fig. 7d). Nevertheless, the formation of bubbles again caused vertical (see yellow dashed line with squares on Fig. 6) as well as horizontal movement of the mud. The formation of icy-muddy crust was also observed at contact with the icy-sandy surface. However, this time the formation of icy-muddy crust did not enhance the vertical movement of the mud as observed in the experiment captured on Fig. 5f-j. When the most vigorous stage of boiling ended (Fig. 6c), a significant volumetric decrease was observed (Fig. 6 and Fig. 7d). The volumetric decrease stopped lateral movement of the mud and was

319 accompanied by a formation of ice crystals on the mud edges (Fig. 7d). These ice crystals slowly grew

320 towards the center of the mud edifice. Firstly, the mud extruded over the icy-sandy surface developed an

321 icy-muddy crust. Subsequently, the crust began to grow toward the central part (Fig. 7e). The maximum

322 volumetric increase reached ~10% for this experimental setup, however, due to the deflation episode the

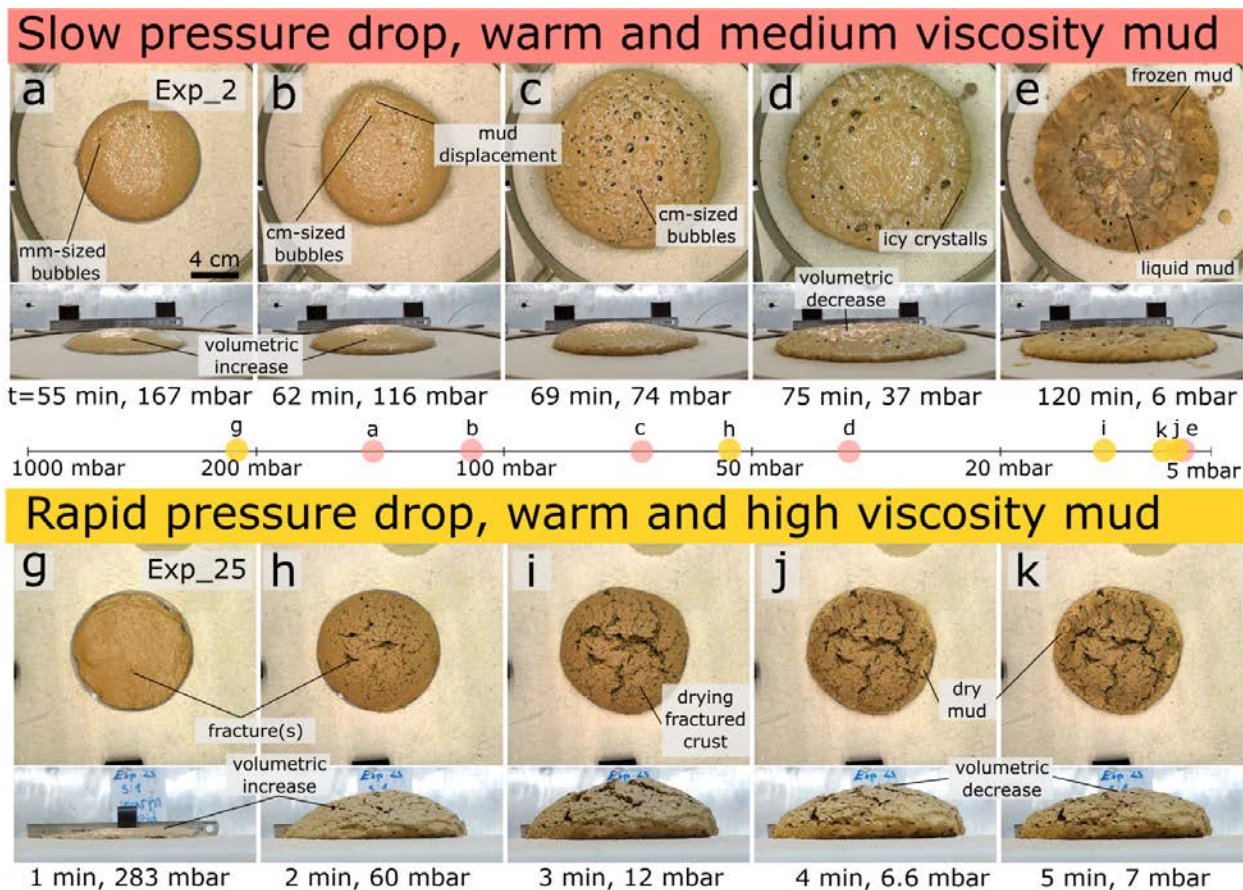323 final volumetric change was only ~6.4% (Fig. 6).

324

325 Figure 7. *A sequence of images from different time steps capturing the behavior of "warm" medium*

326 *viscosity mud (upper sequence) and "warm" high viscosity mud (lower sequence) during the slow and*

327 *rapid pressure drop, respectively. While the medium viscosity mud experienced intense boiling leading to*

328 *significant lateral growth, the high viscosity mud expanded instead in the vertical direction only. Also, the*

329 *high viscosity mud did not show signs of intense boiling and bubble escape, instead, fracturing was*

330 *observed. Each panel is composed by two figures capturing the experiment from above (upper image,*

331   *cam#1) as well as from the side (lower image, cam#2). The axis between the panels shows the pressure*

332   *value and position of each time step is marked there.*

333   ## 3.2 High viscosity mixture

334   For the high viscosity mixture vigorous boiling was not observed during the pressure drop

335   regardless of the temperature of the mud or how fast the pressure drop was. However, as the pressure

336   decreased, the mud volume started to increase (see solid lines with circles on Fig. 6 for details). The mud

337   first responded plastically to the change in volume, however, as the volume change became more

338   significant, small cracks began to appear on the surface of the mud (Figs. 7g,h). These cracks gradually

339   increased in sizes and depths. When surface cracks penetrated deep enough to reach pockets of gas that had

340   accumulated within the mud mixture a partial episode of volumetric decrease was observed. This was

341   followed by a volumetric increase again. Volumetric decrease and increase subsequently alternated for a

342   while, and the movement of the mud thus resembled the movement of a breathing chest. When the pressure

343   fell below ~8 mbar, signs of accelerated mud drying were observed at the edges of the mud body (Figs.

344   7j,k). At this point, deflation became the dominant process and the mud body began to dwindle in size (see

345   red solid lines with circles on Fig. 6). The mud propagation in the lateral direction during this stage was

346   very limited when compared to the experiments using the medium viscosity mud mixtures. When the

347   experiment was terminated and the chamber pressurized again, the part of the muddy body that was inflated

348   above the plastic cup was carefully cut open. This exposed a cavity several centimeters wide trapped under

349   partly dried up and partly frozen muddy fractured crust.

350   The results of different experimental setups for a) medium and high viscosity mud mixtures of b)

351   various temperatures ("cold" and "warm") and c) exposed to differently accelerated pressure drops ("rapid"

352   and "slow") are summarized in Fig. 8. While experiments using high viscosity mud have relatively uniform

353   resulting shapes, this is not the case for experiments conducted using the medium viscosity mud:. The latter

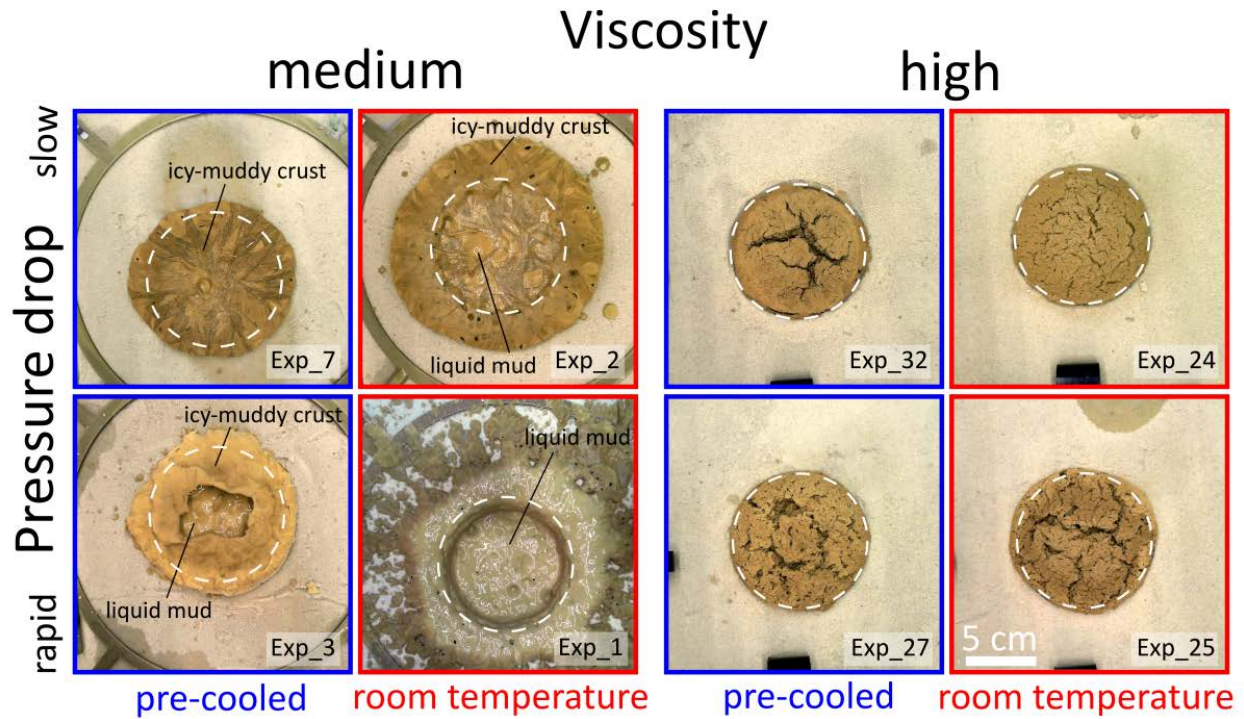354   experiments show much larger variability in resulting shapes.

355

Figure 8: Examples of mud inflation morphologies during pressure decrease experiments. The blue and red boxes mark different mud temperatures. Morphologies of high viscosity mud are relatively uniform. In contrast, a wider variety exists for the less viscous, medium viscosity mud. The white dashed lines denote the position of the 9 cm large container.

Finally, two experiments using the low viscosity mud mixture were performed (see Table 1). These experiments revealed that despite intense boiling caused by instability of water under the reduced atmospheric pressure and subsequent freezing caused by evaporative cooling, no volumetric increase was observed because vapor bubbles escaped easily from the low viscosity mixture. However, intense boiling and bubbling caused a significant ejection of mud droplets into the surrounding area.

4. Discussion

4.1. Behavior of bubbles in mud as a function of viscosity

As shown by our experiments, reduced atmospheric pressure has a profound effect on the mud behavior. In fact, water is not stable when exposed to the reduced pressure – it boils and subsequently freezes near the surface due to evaporative cooling (Bargery et al., 2010). Boiling coupled with the formation of large quantities of variously sized bubbles within the mixture might cause levitation (Raack et al., 2017; Brož et al., 2020b), freezing instead results in a formation of an icy-muddy crust (Brož et al., 2020a). Depending on the viscosity of the mud (Fig. 3), the vapor bubbles either a) rise and escape easily from the mud, b) are significantly slowed down during their ascent, or c) are completely blocked from leaving the mud mixture (Fig. 9). These three different outcomes have a profound effect on the behavior and volumetric change of the mud.
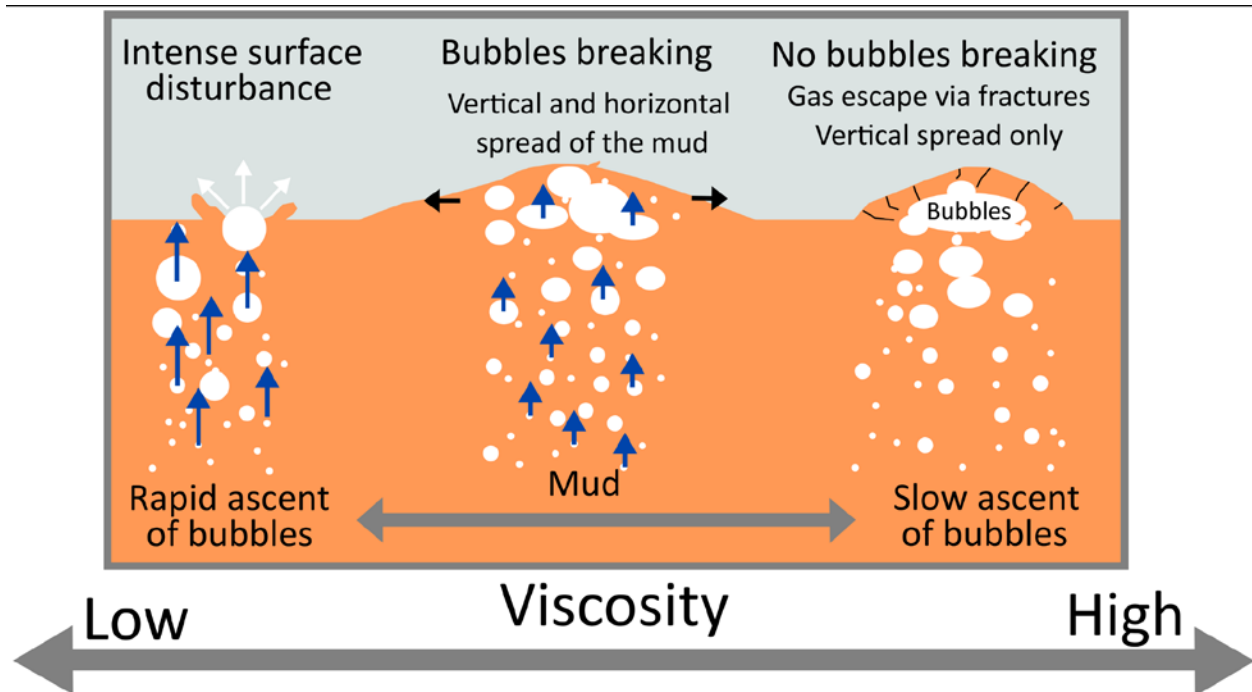

Figure 9: Simplified concept of gas migration and mud inflation due to the pressure drop.

378   When the mud mixture has a low viscosity (75 wt% water and 25 wt% clay, blue line in Figure 3,

379   "low" viscosity) and thus the viscous drag it exerts is small, our experiments show that the bubbles can

380   easily escape through the mud, reaching velocities that result in visible disruptions of the surface. During

381   their rise through the mixture, the bubbles are increasing in volume due to a) ongoing evaporation through

382   the surface of each bubble, b) decrease of hydrostatic pressure that leads to expansion of the gas phase,

383   and/or c) coalescence with other rising bubbles (e.g., Parfitt and Wilson, 2008). At the end of the ascent,

384   we observed centimeter-sized, rapidly escaping bubbles that caused intense surface disturbances (Fig. 9,

385   left scenario) and ejections of mud into the surroundings. This causes a splashing of some quantity of the

386   mud into the surroundings and hence an enhanced lateral distribution of the mud, but no volumetric change

387   within the mud is observed as no bubbles remain trapped within the mixture.

388   When mud viscosity is higher (50 wt% water and 50 wt% clay, green line in Fig. 3, "medium"

389   viscosity), the bubbles' ascent is slower and their escape from the mud is less dynamic. The bubbles' rise

390   velocity can be roughly estimated using Stokes' law, giving ca. 0.1 millimeters per minute for a 2 mm sized

391   spherical bubble in mud of viscosity of 2 Pas. Since the Stokes velocity scales with the square of the particle

392   radius, less than 1 mm-sized bubbles are likely to remain trapped in the mud during the experiment. In

393   contrast, cm-sized bubbles move easily through the medium viscosity mud. After bubbles nucleate within

394   the mixture, they increase in volume due to the evaporation, decompression and coalescence, increasing

395   the overall volume of the mud (Figs. 5 and 7). This causes a primarily vertical growth of the mud, because

396   the body is confined from the sides by the walls of the circular container (Fig. 9, middle scenario). The

397   newly generated volume piles on top of the container and spreads laterally, forming small lobes that are

398   radially propagating around the source area (Fig. 8). The mud in these lobes continues growing in volume,

399   as it is still boiling inside, which is additionally boosting its lateral spread. However, as the thickness of the

400   laterally spreading lobes is relatively small in comparison with the thickness of the parental muddy body,

401   the number of bubbles that can be slowed down and/or trapped within the mud is limited. This reduces

402   additional volumetric increase in these lobes.

403   Finally, when the mud viscosity is even higher (25 wt% water and 75 wt% clay, red line in Fig. 3,

404   "high" viscosity), the movement of vapor bubbles through the mud is negligible. Assuming the viscosity of

405   20 Pas, a spherical bubble with 1 cm in diameter has the Stokes velocity of less than 0.1 mm/min, which

406   means that most of the bubbles would remain in the place of their formation. Moreover, the shear stress

407   generated by the presence of mm-sized bubbles is expected to be on the order of tens of Pascals at

408   maximum, and thus does not exceed the static yield stress of the high viscosity mud (see Supplementary

409   Information). Under such circumstances, the mixture is boiling, but the bubbles are mostly trapped (Fig. 9,

410   right scenario) and their growth is controlled by decompression and coalescence to a lesser extent.

411   Nevertheless, we discovered several centimeter-sized empty voids under less than 1-2 centimeter thick,

412   partly dried up and partly frozen muddy crust. This suggests that vapor is still able to move through the

413   medium from larger cavities. We speculate that these features may be related to the formation of fractures

414   within the high viscosity mud. This network interconnects different gas pockets and allows coalescence of

415   the gas. Due to the high viscosity of the mixture, the lateral movement of the surface mud pile is very

416   limited and the volumetric increase is accommodated predominantly in the vertical direction. This is

417   additionally supported by relatively rapid drying and freezing of the mud, which causes the formation of

418   even more viscous crust hence making more difficult lateral spreading of the mixture. However, at some

419   point the volume of mud may also drop. This is due to the fact that the fractures can break through the area

420   of accumulated gas, causing it to escape from the mixture leading to mud body decrease (full red line in

421   Fig. 6).

422   We deliberately selected the mud viscosity in order to simulate the end-member scenarios. It is

423   clear, however, that in between the three mud types (i.e. the low, medium, and high viscosity) transitions

424   exist during which individual neighboring scenarios approach each other, until finally one prevails over

425   another (Fig. 9). If the water content changes during sediment mobilization (or the resulting viscosity

426   changes for any other reason), the response of the water-mud mixture to reduced atmospheric pressure

427   should change accordingly. This means that the response of the hundreds of meters up to kilometer-long

428   mud flows to reduced atmospheric pressure might differ in different parts of the flow, as the water content

429   within the mud mixture varies due to atmospheric loss or infiltration into the subsurface (depths of boiling

430   that are expected in the natural, large-scale environments are discussed in Section 4.2). Also if the amount

431   of water within the mixture becomes reduced to a certain threshold, we expect the mixture to stop behaving

432   in a viscous manner (e.g. Kelessidis and Maglione, 2008; Abu-Jdayil, 2011). Once such a rheological

433   transition occurs, the here-described mechanisms of volumetric increase would stop operating. We

434   therefore argue that the process of rapid volumetric change is limited only to a certain range of viscosities

435   and might not affect all types of muds expelled by sedimentary volcanism on Mars.

436   Viscosity does not only affect the way in which boiling increases the mud volume, but also the

437   speed of evaporative cooling. Lateral spreading of a highly viscous mud is limited, reducing the area that

438   cools evaporatively due to the exposure to low pressure conditions. Consequently, mud flows that spread

439   easily over the surface should cool down quicker than the narrower flows formed by higher viscosity muds.

440   Note that the laterally spreading mud is freezing from the top (due to evaporative cooling), as well

441   as from the bottom due to contact with the ice-sand layer. In the slow pressure drop experiments, conductive

442   cooling results in the freezing of several millimeters of the mud, which explains why material that is outside

443   of the container is more likely to be frozen at the end of each experiment (see, e.g., Fig. 7e). We do not

444   focus on distinguishing between the two cooling mechanisms because both the conductive and evaporative

445   cooling are more efficient when the mud spreads over a larger area. Both these mechanisms promote the

446   formation of icy-muddy crust that inhibits further mud spreading.

447   To conclude, the performed experiments highlight the difference in behavior between centimeter-

448   to decimetre-thick mud flows on the surface of Mars and Earth. The pT conditions on Earth to which mud

449   is released are within the range of water stability – in most common scenarios, mud is extruded on Earth to

450   conditions that do not trigger boiling. Hence, extrusions are not accompanied by a formation of large

451   quantities of bubbles that could become trapped inside the mud. Centimetre- to decimetre-thick mud flows

452   on Earth hence do not show significant volumetric changes during their movement over the surface, and

453   hence their final morphologies can be modeled in steady uniform regime. On the other hand, putative

454   martian centimeter- to decimetre-thick mud flows would behave very differently on present-day Mars

455   conditions. Although the exact evolution of martian atmospheric pressure over time is not well understood,

456   it is generally agreed that the paleopressure over the Amazonian period remained low (Kite et al., 2014),

457   suggesting possible applicability of our results also to some of the ancient mud flows. We support the

458   previous notions that sedimentary edifices built by accumulation of mud on Mars might have significant

459   variations in their shapes and morphologies from terrestrial counterparts (e.g., Brož et al., 2019, 2020a,b,

460   2022, 2023; Cuřín et al., 2023). This is because the atmospheric pressure of Mars gives rise to several

461   processes linked with water instability that do not operate on Earth. This leads us to predict that when the

462   same volume of mud is extruded on Earth and Mars, the resulting mud flow on Mars will have a higher

463   thickness and porosity than the terrestrial counterpart, and will likely be narrower due to the formation of

464   an icy-muddy crust.

4.2. Limitations and implications

466   Currently known putative martian mud-volcanoes are much larger, with observable mud flow

467   thicknesses of several meters or more, than observed in our experiments. In this section we discuss the

468   extrapolation of our results to larger scales.

469   The mud weight inside the container increases the hydrostatic pressure as a function of depth. At a

470   certain depth, the pressure reaches the equilibrium vapor pressure, that is, no bubbles form below that depth

471   even though the atmospheric pressure is low. For a 20°C mud of density 1500 kg/m^3, the depth of boiling

472   is 15 cm at terrestrial surface gravity, i.e. it exceeds the depth of our container (cf. Fig. 2). In a meter-deep

473   container only the top part would participate in the processes that we describe, and the relative volume

474   change would thus be smaller. In other words, the values provided in Fig. 6 represent the relative volumetric

475   change of the boiling layer in the container. Moreover, the size distribution of bubbles inside the mud is not

476   uniform. Their nucleation frequency increases toward the surface and they grow in size along their paths

477 through the liquid mud. The resulting size distribution is non-uniform, with more gas residing in the shallow

478 parts. We measure the relative change of volume of mud in the 8 cm deep container, and our results are

479 thus only a rough estimate of what the volumetric change of the boiling layer is. The primary aim here is

480 to qualitatively map the behavior of end-member scenarios.

481   On Mars, the surface gravity is nearly three times smaller than on Earth, which makes the depth of

482 boiling nearly three times larger, reaching meters for sufficiently warm muds (Fig. 10). This leads us to

483 conclude that the observed mounds associated with putative martian mud-volcano-like edifices might

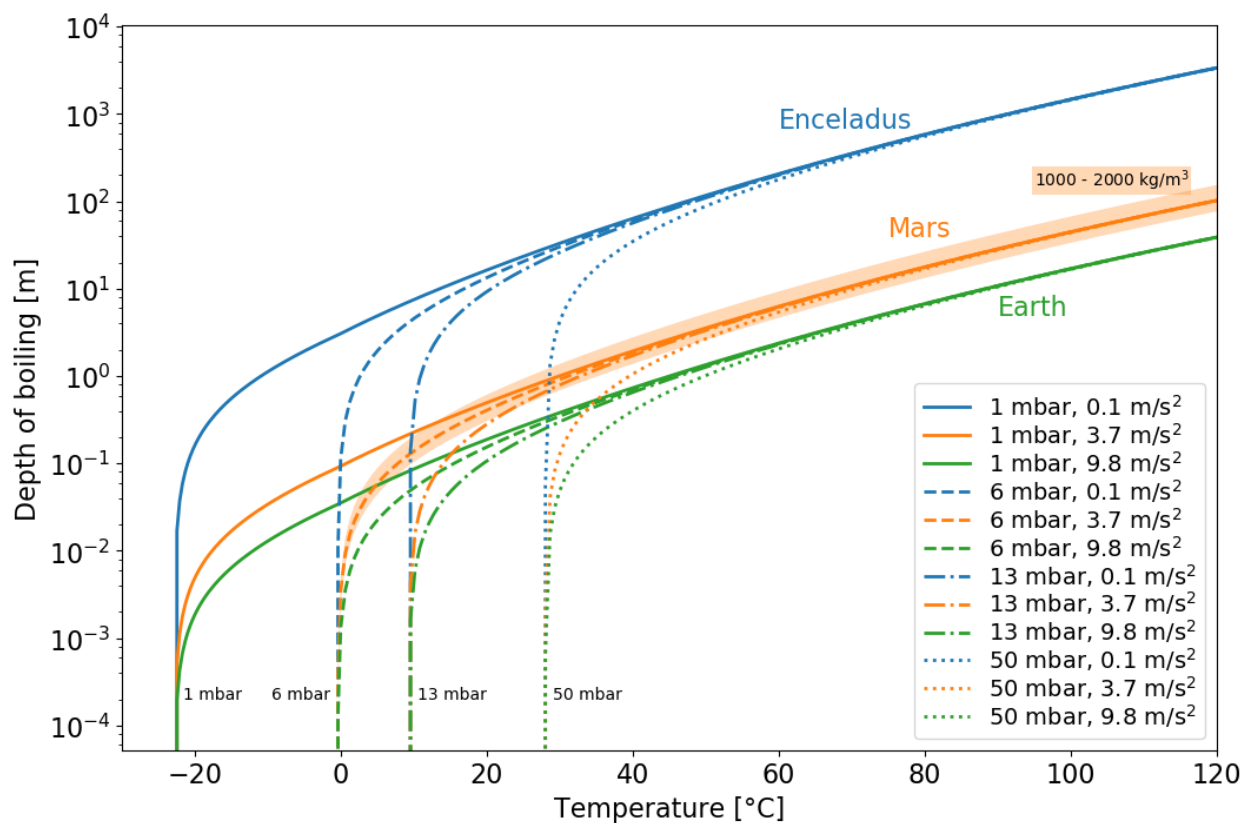484 indeed be formed by the process of volumetric increase.

485

486   *Figure 10: Influence of surface gravity and atmospheric pressure on the depth of boiling. Assuming*

487 *hydrostatic pressure in the mud, we compute the depth at which the water component becomes stable,*

488 *varying both the atmospheric pressure (1, 6, 13, and 50 mbar) and the value of the gravitational*

489 *acceleration (Earth: green, Mars: orange, and Enceladus: blue). Mud density is set to 1500 kg/m^3 in all*

490   *cases, for atmospheric pressure of 7 mbar and the surface gravity of Mars the mud density is varied in the*

491   *range of 1000 and 2000 kg/m³ (orange shaded region). The equilibrium vapor pressure is obtained from*

492   *Bohren and Albrecht (1998).*

493   As the temperature of the mud decreases, the equilibrium vapor pressure approaches the atmospheric

494   pressure on Mars. When the mud temperature is 1°C, the depth of boiling is less than a centimeter under

495   Earth's gravity. Boiling can quickly propagate deeper because the formed bubbles significantly reduce the

496   density of the mixture, decreasing the hydrostatic pressure in effect (cf. the orange shaded region in Fig.

497   10), but it is still likely that only a shallow part of the container was in fact boiling in the experiments in

498   which mud was pre-cooled. For cold muds, the relative change of volume of the boiling layer may exceed

499   the values measured for the full container (Fig. 6), but the boiling layer is also very thin. Note that salts and

500   impurities increase the boiling temperature of water and thus reduce the depth of boiling - the values

501   provided in Fig. 10 are the upper estimate.

502   A mixture of clay with water may become mobilized also on other planetary bodies. For example,

503   the presence of a large muddy body was proposed on Ceres (Ruesch et al., 2019) that has even lower surface

504   gravity than Mars and near vacuum atmosphere, i.e. conditions that imply deep, vigorous boiling.

505   Additionally, as the process of volumetric increase caused by rapid bubble growth due to the low pressure

506   conditions was initially proposed in association with lunar lavas by Wilson and Head (2017), we suggest

507   that other types of liquids might show similar behavior as experiments with mud. The key requirements are

508   only that the liquid is unstable in the low pressure environment and that its viscosity is high enough to

509   impede and eventually trap the gas bubbles. For example, cryovolcanism during which the liquid water is

510   effused to near vacuum environment on icy moons (e.g. Enceladus or Europa) might reach sufficient

511   viscosities if the amount of crystals within the mixture is high enough to reach the rheological transition.

512   As shown in Fig. 10, the depth of boiling increases by two orders of magnitude on Enceladus when

513   compared to Earth, because the surface gravity is by two orders of magnitude smaller. It is currently

514   unknown if water effused during cryovolcanism increases in viscosity to levels such as to reach the critical

515 threshold for the volumetric change to operate, however, if so, this process might lead to observational

516 evidence on its surface as well.

517   Both the depth of boiling and the ascent velocity of bubbles are affected by the value of surface

518 gravity. The Stokes velocity, which is a proxy for the ascent velocity, depends linearly on the value of g.

519 On a body like Enceladus, with a hundred times smaller gravity, bubbles would take much longer to reach

520 the surface than in our experiments. This could moderate the effect of boiling such that even a low-viscosity

521 material could impede the bubbles significantly, which means that mixtures of the same viscosity may

522 behave differently under different surface gravities

5. Conclusions

524 Our experiments show that low atmospheric pressure has a profound effect on the behavior of muds

525 with viscosities higher than ~1 Pas. The instability of water results in boiling and thus formation of large

526 quantities of bubbles (Bargery et al., 2010) that can migrate from the mud mixture with different pacing.

527 Furthermore, the low pressure conditions trigger evaporative cooling of the mud, and hence the formation

528 of a frozen crust - this phenomenon inhibits the ability of bubbles to escape from the mixture (Brož et al.,

529 2020a). The retention of bubbles within the mud prompts a volumetric change of the mixture that,

530 depending on the viscosity, can reach up to 30% increase of the sample volume. The observed mechanism

531 bears resemblance to the volumetric changes associated with the degassing of terrestrial lavas or mud

532 volcano eruptions caused by a rapid pressure drop. Our measurements demonstrate that low pressure

533 conditions have important implications in controlling the morphology of the mud edifices formed by

534 eruptive events.

535 The surface gravity on Mars is nearly three times smaller than that on Earth, and the layer of mud that

536 undergoes boiling is thus thicker on Mars. As a consequence, the boiling observed during our small scale

537 experiments may apply to larger scales in the natural conditions on Mars. This suggests that the observed

538 mounds and knobs associated with putative martian sedimentary volcanoes might indeed be related to mud

volumetric changes in response to surface exposure. We also suggest that other types of liquid that are unstable in the low pressure environment might show similar behavior if their viscosity is high enough to prevent the bubble escape. The results presented herein have implications also for cryovolcanic phenomena on icy moons (e.g. Enceladus or Europa) or dwarf planets like Ceres. Since these bodies have surface gravities two orders of magnitude smaller than Earth or Mars, boiling can be expected to occur at even larger depths and hence be a crucial factor in controlling the surface morphologies after eruptive processes.

6. Acknowledgments

7. Availability Statement

The movies and temper-ature and pressure data that support the findings of this study are available in Zenodo .orgwith the identifier 8016218 (https://zenodo.org/record/8016218).

8. References

Abu-Jdayil, B. (2011). Rheology of sodium and calcium bentonite–water dispersions: Effect of electrolytes and aging time. *International journal of mineral processing*, 98(3-4), 208-213. https://doi.org/10.1016/j.minpro.2011.01.001

Bargery, A.S., Lane, S.J., Barrett, A., Wilson, L., Gilbert, J.S. (2010). The initial responses of hot liquid water released under low atmospheric pressures: experimental in-sights. *Icarus,* 210(1), 488–506. https://doi.org/10.1016/j.icarus.2010.06.019

562 Bohren, F.C., & Albrecht, A.A. (1998). Atmospheric Thermodynamics, Oxford University Press, New
563   York. ISBN 0-19-509904-4

564 Brož, P., Hauber, E., van de Burgt, I., Špillar, V., and Michael, G. (2019). Subsurface sediment mobilization
565   in the southern Chryse Planitia on Mars. *Journal of Geophysical Research*, 124, 703-720.
566   https://doi.org/10.1029/2018JE005868

567 Brož, P., Krýza, O., Wilson, L., Conway, S.J., Hauber, E., Mazzini, A., Raack, J., Patel, M. R., Balme,
568   M.R., Sylvest, M.E. (2020a). Experimental evidence for lava-like mud flows under Martian surface
569   conditions. *Nature Geoscience*, 13, 403-407. https://doi.org/10.1038/s41561-020-0577-2.

570 Brož, P., Krýza, O., Conway, S.J., Mueller, N.T., Hauber, E., Mazzini, A., Raack, J., Patel, M.R., Balme,
571   M.R., Sylvest, M.E. (2020b). Mud flow levitation on Mars: insights from laboratory simulations.
572   *EPSL*, 545. https://doi.org/10.1016/j.epsl.2020.116406

573 Brož, P., Bernhardt, H., Conway, S. J., Parekh, R. (2021). An overview of explosive volcanism on Mars.
574   J*ournal of Volcanology and Geothermal Research,* 409, 107125.
575   https://doi.org/10.1016/j.jvolgeores.2020.107125

576 Brož, P., Hauber, E., Conway, S.J., Luzzi, E., Mazzini, A., Noblet, A., Jaroš, J., Fawdon, P., and Markonis,
577   Y. (2022). New Evidence for Sedimentary Volcanism on Chryse Planitia, Mars. *Icarus* 382, 115038.
578   https://doi.org/10.1016/j.icarus.2022.115038

579 Brož, P., Oehler, D., Mazzini, A., Hauber, E., Komatsu, G., Etiope, G., Cuřín, V. (under review). An
580   overview of sedimentary volcanism on Mars, *ESURF*, EGUsphere [preprint, available online].
581   https://doi.org/10.5194/egusphere-2022-1458

582 Chassefiére, E., & Leblanc, F. (2011). Methane release and the carbon cycle on Mars. *Planetary and Space*
583   *Science*, 59, 207–217. https://doi.org/10.1016/j.pss.2010.09.004

584 Clark, B.C. (1978). Implications of abundant hygroscopic minerals in the Martian regolith. *Icarus*, 34, 645–

585   665. https://doi .org /10.1016/0019-1035(78)90052-0

586 Corradi, A.B., Manfredini, T., Pellacani, G.C., Pozzi, P. (1994). Deflocculation of concen-trated aqueous

587   clay suspensions with sodium polymethacrylates. *Journal of the American Ceramic Society*, 77 (2).

588   https://doi.org/10.1111/j.1151-2916.1994.tb07022.x

589 Cuřín, V., Brož, P., Hauber, E., Markonis, Y. (2023). Mud flows in Southwestern Utopia Planitia, Mars.

590   *Icarus*, 389. https://doi.org/10.1016/j.icarus.2022.115266

591 De Toffoli, B., Massironi, M., Mazzarini, F., Bistacchi, A. (2021). Rheological and mechanical layering of

592   the crust underneath thumbprint terrains in Arcadia Planitia, Mars. *Journal of Geophysical Research:*

593   *Planets,* 126. https://doi.org/10.1029/2021JE007007e2021JE007007

594 De Toffoli, B., Pozzobon, R., Massironi, M., Mazzarini, F., Conway, S., Cremonese, G. (2019). Surface

595   expressions of subsurface sediment mobilization rooted into a gas hydrate-rich cryosphere on Mars.

596   *Scientific Reports,* 9, 8603. https://doi.org/10.1038/s41598-019-45057-7

597 Hecht, M.H. (2002). Metastability of liquid water on Mars. *Icarus,* 156, 373–386.

598   https://doi.org/10.1006/icar.2001.6794.

599 Hecht, M.H., et al., (2009). Detection of perchlorate and the soluble chemistry of mar-tian soil at the

600   Phoenix lander site. *Science,* 325, 64–67. https://doi .org /10 .1126 /science .1172466

601 Kite, E. S., Williams, J.-P., Lucas, A., Aharonson, O. (2014). Low palaeopressure of the martian atmosphere

602   estimated from the size distribution of ancient craters. *Nature Geoscience*, 7, 335–339,

603   https://doi.org/10.1038/ngeo2137

604 Kelessidis, V. C., & Maglione, R. (2008). Yield stress of water–bentonite dispersions. *Colloids and*

605   *Surfaces A: Physicochemical and Engineering Aspects*, *318*(1-3), 217-226.

606   https://doi.org/10.1016/j.colsurfa.2007.12.050

607   Laigle, D., & Coussot, P. (1997). Numerical modelling of mudflows. *Journal of Hydraulic Engineering*,

608   123, 617–623. https://doi.org/10.1061/(ASCE)0733-9429(1997)123:7(617)

609   Mazzini, A., & Etiope, G. (2017). Mud volcanism: an updated review. *Earth-Science Reviews,* 168, 81–

610   112. https://doi.org/10.1016/j.earscirev.2017.03.001

611   McGowan, E. (2011). The Utopia/Isidis overlap: possible conduit for mud volcanism on Mars. *Icarus*, 212,

612   622–628. https://doi.org/10.1016/j.icarus.2011.01.025

613   O'Brien, J.S., & Julien, P.Y. (1988). Laboratory analysis of mudflow properties. *Journal of Hydraulic*

614   *Engineering*, 114, 877–887. https://doi.org/10.1061/(ASCE)0733-9429(1988)114:8(877)

615   Parfitt, E.A., & Wilson, L. (2008). Fundamentals of Physical Volcanology, 256 pp. Blackwell, Oxford, U.

616   K.

617   Raack, J., Conway, S.J., Herny, C., Balme, M.R., Carpy, S., Patel, M.R. (2017). Water-induced sediment

618   levitation enhances downslope transport on Mars. *Nature Communications*, 8.

619   https://doi.org/10.1038/s41467-017-01213-z

620   Ruesch, O., Genova, A., Neumann, W., Quick, L.C., Castillo-Rogez, J.C., Raymond, C.A., Russel, Ch.T.,

621   Zuber, M.T. (2019). Slurry extrusion on Ceres from a convective mud-bearing mantle. *Nature*

622   *Geoscience*, 12, 505–509. https://doi.org/10.1038/s41561-019-0378-7

623   Thielicke, W., & Stamhuis, E. (2014). PIVlab–towards user-friendly, affordable and accurate digital

624   particle image velocimetry in MATLAB. *Journal of open research software*, 2(1).

625   https://doi.org/10.5334/jors.bl

626   Vaniman, D.T., Bish, D.L., Chipewa, S.J., Fialips, C.I., Carrey, J.W., Feldman, W.C. (2004). Magnesium

627   sulphate salts and the history of water on Mars. *Nature*, 431, 663–665.

628   https://doi.org/10.1038/nature02973

629   Wilson, L., & Head, J.W. (2017). Eruption of magmatic foams on the moon: formation in the waning stages

630   of dike emplacement events as an explanation of "irregular mare patches". *Journal of Volcanology*

631   *and Geothermal Research*, 335, 113–127. https://doi.org/10.1016/j.jvolgeores.2017.02.009

632   Wilson, L., & Mouginis-Mark, P. J. (2014). Dynamics of a fluid flow on Mars: Lava or mud? *Icarus,* 233,

633   268–280. https://doi.org/10.1016/j.icarus.2014.01.041, 2014

634